Article

Binary Nanoparticle Superlattices in the Semiconductor–Semiconductor System: CdTe and CdSe

Zhuoying Chen, Jenny Moore, Guillaume Radtke, Henning Sirringhaus, and Stephen O'Brien

J. Am. Chem. Soc., **2007**, 129 (50), 15702-15709 • DOI: 10.1021/ja076698z

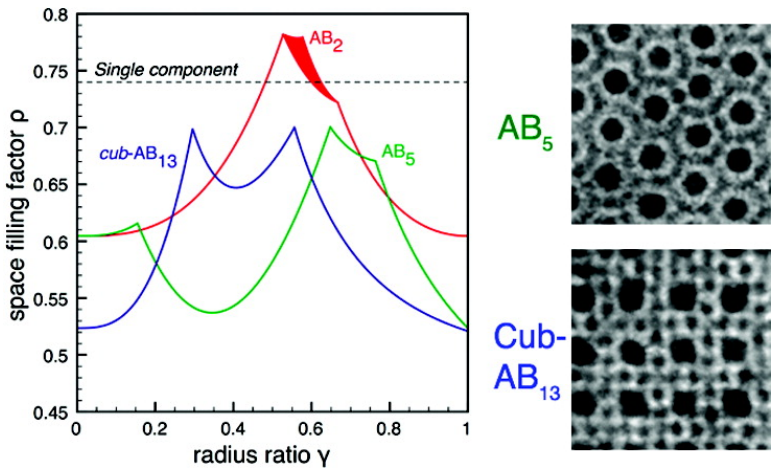

More About This Article

Additional resources and features associated with this article are available within the HTML version:

- Supporting Information
- Links to the 5 articles that cite this article, as of the time of this article download
- Access to high resolution figures
- Links to articles and content related to this article
- Copyright permission to reproduce figures and/or text from this article

View the Full Text HTML

J|A|C|S
ARTICLES
Published on Web 11/23/2007

Binary Nanoparticle Superlattices in the Semiconductor−Semiconductor System: CdTe and CdSe

Zhuoying Chen,[†] Jenny Moore,[‡] Guillaume Radtke,[§] Henning Sirringhaus,[‡] and Stephen O'Brien*,[†]

Contribution from the Department of Applied Physics & Applied Mathematics, Columbia University, 200 SW Mudd Building, 500 W 120th Street, New York, New York 10027, University of Cambridge, Cavendish Lab, Cambridge CB3 0HE, UK, and Laboratoire TECSEN, UMR 6122 CNRS, Faculté des Sciences de Saint-Jérôme, case 262, Université Paul Cézanne-Aix Marseille III, 13397 Marseille cedex 20, France

Received September 5, 2007; E-mail: so188@columbia.edu

Abstract: We report binary nanoparticle superlattices obtained by self-assembly of two different semiconductor quantum dots. Such a system is a means to include two discretized, quantum-confined, and complimentary semiconductor units in close proximity, for purposes of band gap matching and/or energy transfer. From a range of possible structures predicted, we observe an exclusive preference for the formation of Cuboctahedral AB_{13} and AB_5 (isostructural with $CaCu_5$) obtained in the system of 8.1 nm CdTe and 4.4 nm CdSe nanoparticles. For this system, a possible ionic origin for the formation of structures with lower packing densities was ruled out on the basis of electrophoretic mobility measurements. To understand further the principles of superlattice formation, we constructed space-filling curves for binary component hard spheres over the full range of radius ratio. In addition, the pair interaction energies due to core−core and ligand−ligand van der Waals (VDW) forces are estimated. The real structures are believed to form under a combined influence of entropic driving forces (following hard-sphere space filling principles) and the surface (due to ligand−ligand VDW).

Introduction

Self-organization or self-assembly of binary components of large and small colloidal particles has aroused much interest in materials science since the early 1980s.[1−3] Recently, due to the progress in colloidal synthetic techniques,[4−9] the colloidal components for self-assembly have been extended from micrometer-sized hard spheres (e.g., silica[2,10,11] or latex[1] or polymethylmethacrylate (PMMA)[11−17] spheres) to nanometer-sized nanoparticles (NPs) that can be of different intrinsic properties (e.g., semiconductor NPs self-assembled with metal oxide NPs,[18] or semiconductor NPs with metal NPs[19−21]). Self-assembly for ordered multicomponent nanoparticle superlattices not only provides opportunities to probe the unique physics of self-assembling in the nanometer scale but also can potentially be utilized as a "bottom-up" design tool to build "metamaterials" of novel physical properties distinct from their individual components.[18−21] However, the formation mechanism of multicomponent self-assembly of nanoparticles is still not yet well understood. In addition to formation kinetics, the self-assembly of multicomponent nanoparticles can involve a complex balance between different driving forces such as entropy, Coulomb interaction from particle charges, London-van der Waals forces, charge−dipole interaction, and dipole−dipole interactions.[20,22−24] Therefore, for self-assembly to be really utilized as an effective

[†] Columbia University.
[‡] University of Cambridge.
[§] Université Paul Cézanne-Aix Marseille III.

(1) Hachisu, S.; Yoshimura, S. *Nature* **1980**, *283*, 188−189.
(2) Murray, M. J.; Sanders, J. V. *Philos. Mag. A* **1980**, *42*, 721−740.
(3) Sanders, J. V. *Philos. Mag. A* **1980**, *42*, 705−720.
(4) Steigerwald, M. L.; Alivisatos, A. P.; Gibson, J. M.; Harris, T. D.; Kortan, R.; Muller, A. J.; Thayer, A. M.; Duncan, T. M.; Douglass, D. C.; Brus, L. E. *J. Am. Chem. Soc.* **1988**, *110*, 3046−3050.
(5) Steigerwald, M. L.; Brus, L. E. *Ann. Rev. Mater. Sci.* **1989**, *19*, 471−495.
(6) Murray, C. B.; Norris, D. J.; Bawendi, M. G. *J. Am. Chem. Soc.* **1993**, *115*, 8706−8715.
(7) Brust, M.; Walker, M.; Bethell, D.; Schiffrin, D. J.; Whyman, R. *J. Chem. Soc. Chem. Commun.* **1994**, 801−802.
(8) Motte, L.; Billoudet, F.; Pileni, M. P. *J. Phys. Chem.* **1995**, *99*, 16425−16429.
(9) Murray, C. B.; Kagan, C. R.; Bawendi, M. G. *Science* **1995**, *270*, 1335−1338.
(10) Yethiraj, A.; Thijssen, J. H. J.; Wouterse, A.; van Blaaderen, A. *Adv. Mater.* **2004**, *16*, 596.
(11) Cho, Y. S.; Yi, G. R.; Lim, J. M.; Kim, S. H.; Manoharan, V. N.; Pine, D. J.; Yang, S. M. *J. Am. Chem. Soc.* **2005**, *127*, 15968−15975.
(12) Bartlett, P.; Ottewill, R. H.; Pusey, P. N. *Phys. Rev. Lett.* **1992**, *68*, 3801−3804.
(13) Bartlett, P.; Pusey, P. N. *Phys. A* **1993**, *194*, 415−423.
(14) Bartlett, P.; Campbell, A. I. *Phys. Rev. Lett.* **2005**, *95*.
(15) Leunissen, M. E.; Christova, C. G.; Hynninen, A. P.; Royall, C. P.; Campbell, A. I.; Imhof, A.; Dijkstra, M.; van Roij, R.; van Blaaderen, A. *Nature* **2005**, *437*, 235−240.
(16) Hynninen, A. P.; Christova, C. G.; van Roij, R.; van Blaaderen, A.; Dijkstra, M. *Phys. Rev. Lett.* **2006**, *96*.
(17) Hynninen, A. P.; Leunissen, M. E.; van Blaaderen, A.; Dijkstra, M. *Phys. Rev. Lett.* **2006**, *96*.
(18) Redl, F. X.; Cho, K. S.; Murray, C. B.; O'Brien, S. *Nature* **2003**, *423*, 968−971.
(19) Shevchenko, E. V.; Talapin, D. V.; O'Brien, S.; Murray, C. B. *J. Am. Chem. Soc.* **2005**, *127*, 8741−8747.
(20) Shevchenko, E. V.; Talapin, D. V.; Kotov, N. A.; O'Brien, S.; Murray, C. B. *Nature* **2006**, *439*, 55−59.
(21) Shevchenko, E. V.; Talapin, D. V.; Murray, C. B.; O'Brien, S. *J. Am. Chem. Soc.* **2006**, *128*, 3620−3637.
(22) Talapin, D. V.; Shevchenko, E. V.; Murray, C. B.; Titov, A. V.; Kral, P. *Nano Lett.* **2007**, *7*, 1213−1219.
(23) Landman, U.; Luedtke, W. D. *Faraday Discuss.* **2004**, *125*, 22.

10.1021/ja076698z CCC: $37.00

modern method in the nanoscale to design and build superlattices of novel properties, much effort is required to understand the formation mechanism.

In this work, we demonstrate the formation of binary nanoparticle superlattices (BNSLs) in a semiconductor−semiconductor (CdTe and CdSe) system. The choice of this system was motivated by both practical and fundamental interests. Practically, due to the quantum confinement effect in semiconductor nanoparticles, it is possible to adjust the band gap of the particles by adjusting the nanoparticle size during synthesis.[4−6,25,26] Fundamentally, by carefully choosing the nanoparticles, the band offsets at the heterojunction can be tuned and the superlattice metamaterials formed might exhibit interesting charge transport, light-emitting, or light-sensing properties for applications such as solar cells.[27−29] Most currently cited BNSL examples are demonstrated for metal−metal,[30,31] transition metal oxide−semiconductor,[18] and semiconductor−metal[19−21] systems. The observation of BNSLs in the semiconductor−semiconductor system and the discussion of their formation in terms of different driving forces in this work can give further insight into the mechanism of self-assembly at the nanoscale and provide useful information for the future design of metamaterials for practical applications.

Results and Discussion

Nanoparticle and Binary Nanoparticle Superlattices Characterization. In this work, we focus on the semiconductor−semiconductor system of CdTe (core diameter 8.1 nm) and CdSe (core diameter 4.4 nm) nanoparticles (Figure 1). The ligands used in the CdTe nanoparticle synthesis include octadecylphosphonic acid (ODPA) and trioctylphosphine oxide (TOPO), whereas in the CdSe synthesis they are stearic acid, TOPO, and octadecylamine (ODA). Detailed synthetic procedures for these nanoparticles are described in the experimental section (section 4). In both cases, the shape of the particles can be roughly approximated by a sphere. The standard deviation of nanoparticle diameters was determined to be 4.5 and 5.9% for CdTe and CdSe, respectively. Average nanoparticle diameter and diameter distribution were determined by measuring the diameters of 100 nanoparticles in a typical transmission electron microscopy (TEM) image of each system. We measured the thickness of the organic stabilizer shell by analyzing the single component FCC packing TEM images in each nanoparticle system on the [011] or [111] zone axis for the interparticle separation distance along the ⟨110⟩ directions (the close-packed direction). The spacing between the neighbors in the close-packed direction of a nanoparticle array is considered to be twice the thickness of the organic ligand shell.[19,21] From TEM, the thickness of the ligand shell for our CdTe and CdSe nanoparticles is estimated to average ∼0.8 nm. These values are in good

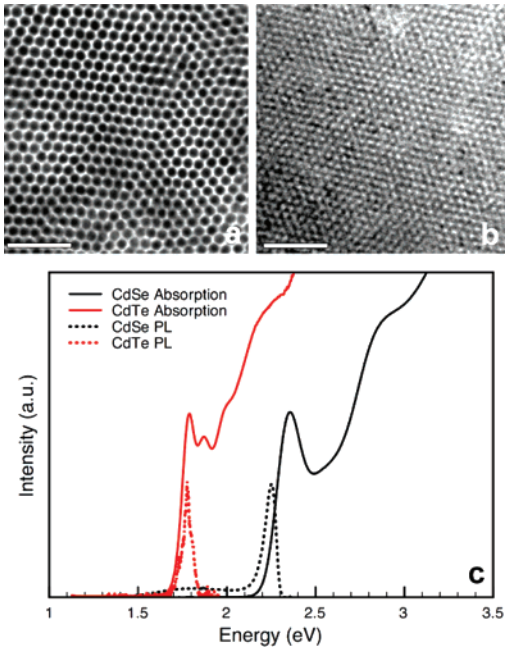

Figure 1. TEM overview of single component superlattices formed by (a) 8.1 nm CdTe and (b) 4.4 nm CdSe nanoparticles under conditions used to grow binary superlattices. All scale bars represent 50 nm. (c) UV−vis absorption and photoluminescence (PL) spectra of 8.1 nm CdTe (red curves) and 4.4 nm CdSe (black curves) nanoparticle solution in toluene.

agreement with those obtained for similar semiconductor nanoparticle systems.[21] The *effective particle diameter*, defined as the diameter of the inorganic core plus twice the thickness of the organic ligand shell,[21] is calculated to be 9.7 nm for our CdTe nanoparticles and 6 nm for CdSe. In the remainder of this work, we will use these effective particle diameters and the size ratio derived from them ($\gamma = d_{\mathrm{Beff}}/d_{\mathrm{Aeff}} = 6/9.7 \approx 0.62$) for our discussion. UV−vis absorption and photoluminescence (PL) measurements were performed on nanoparticle toluene solutions for each system (Figure 1c). The data is consistent with the expected optical properties of 8.1 nm CdTe and 4.4 nm CdSe nanoparticles.[26,32,33]

Two types of superlattice structures, cuboctahedral-AB_{13} (*cub*-AB_{13}) and AB_5 isostructural with intermetallic alloy $CaCu_5$, were observed on substrates suitable for TEM analysis (Cu grids backed with amorphous carbon film) after slow drying the binary nanocrystal solution with a proper CdTe:CdSe concentration ratio (see section 4). The corresponding crystal structures are displayed in Figure 2. The *cub*-AB_{13} structure can be described as a simple cubic lattice with the A particles located at the corners of the cube and with the B particles occupying two inequivalent positions: a B_I particle at the body center of the cube is surrounded by twelve B_{II} particles forming a regular cuboctahedron. This structure is related to the $NaZn_{13}$ (icosahedral-AB_{13} or *ico*-AB_{13}) structure[34] where the cuboctahedron is distorted into an icosahedron. Due to this distortion, the unit cell of the *ico*-AB_{13} is described by a $2 \times 2 \times 2$ arrangement of these cubic sub-cells in such a way that the adjacent icosahedrons are twisted by 90° with respect to each other. This

(24) Mueggenburg, K. E.; Lin, X.-M.; Goldsmith, R. H.; Jaeger, H. M. *Nat. Mater.* **2007**, *6*, 656−660.
(25) Rossetti, R.; Brus, L. *J. Phys. Chem.* **1982**, *86*, 4470−4472.
(26) Murray, C. B.; Kagan, C. R.; Bawendi, M. G. *Ann. Rev. Mater. Sci.* **2000**, *30*, 545−610.
(27) Arici, E.; Meissner, D.; Schaffler, F.; Sariciftci, N. S. *Int. J. Photoenergy* **2003**, *5*, 199−208.
(28) Gregg, B. A.; Hanna, M. C. *J. Appl. Phys.* **2003**, *93*, 3605−3614.
(29) Gledhill, S. E.; Scott, B.; Gregg, B. A. *J. Mater. Res.* **2005**, *20*, 3167−3179.
(30) Kiely, C. J.; Fink, J.; Zheng, J. G.; Brust, M.; Bethell, D.; Schiffrin, D. J. *Adv. Mater.* **2000**, *12*, 640.
(31) Kalsin, A. M.; Fialkowski, M.; Paszewski, M.; Smoukov, S. K.; Bishop, K. J. M.; Grzybowski, B. A. *Science* **2006**, *312*, 420−424.
(32) Talapin, D. V.; Haubold, S.; Rogach, A. L.; Kornowski, A.; Haase, M.; Weller, H. *J. Phys. Chem. B* **2001**, *105*, 2260−2263.
(33) Yu, W. W.; Wang, Y. A.; Peng, X. G. *Chem. Mater.* **2003**, *15*, 4300−4308.
(34) Shoemaker, D. P.; Marsh, R. E.; Ewing, F. J.; Pauling, L. *Acta Crystallogr.* **1952**, *5*, 637−644.

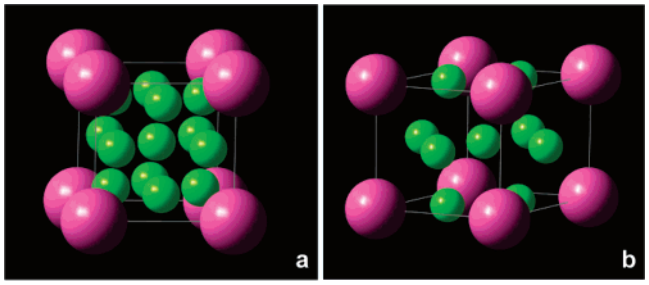

Figure 2. Structure models of (a) *cub*-AB_{13} and (b) $CaCu_5$ structures.

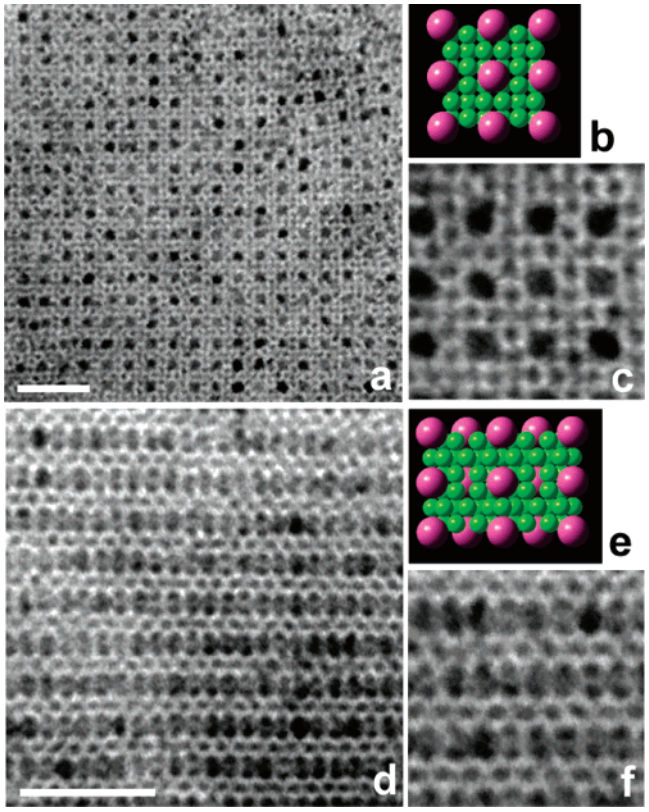

Figure 3. TEM images of the *cub*-AB_{13} superlattices in the (a, b, c) $[001]_{sl}$ and (d, e, f) $[110]_{sl}$ zone axis. (a) and (d) Large view TEM images. (b) and (e) Structural model in the respective zone axis. (c) and (f) Details of the nanoparticle arrangements. All scale bars represent 50 nm.

arrangement gives rise to a much larger unit cell of 112 particles. The AB_5 structure, isostructural with the $CaCu_5$ crystal,[35] can be described as a simple hexagonal lattice of A particles. These A particles are surrounded by a regular arrangement of six B_I particles occupying the trigonal prismatic interstices of the basal planes. An intermediate layer at $z = 1/2$ is formed by the B_{II} particles only, in a Kagomé-type arrangement.

TEM images of the AB_{13} superlattice in the $[001]_{sl}$ and $[110]_{sl}$ zone axis obtained after slow drying the binary solution with the CdTe:CdSe concentration ratio ~1:13 and 1:16 are shown in Figure 3. These two projections lead to an unambiguous identification of the cuboctahedral polytype of this structure.[19] Detailed views (Figure 3c and 3f) of the experimental images obtained in these two zone axes show an excellent agreement with the crystal model displayed in the same figure. The lateral dimensions of the *cub*-AB_{13} superlattices observed on TEM grids are ~0.5 μm × 0.5 μm. Even though the growth directions

(35) Haucke, W. *Z. Anorg. Allg. Chem.* **1940**, *244*, 17−22.

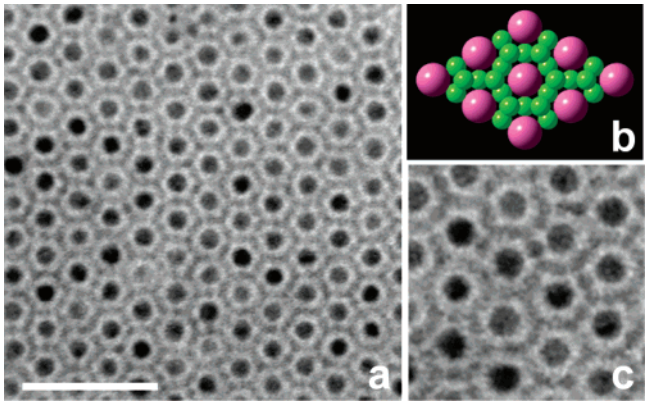

Figure 4. TEM images of the AB_5 superlattices isostructural with $CaCu_5$ in the $[001]_{sl}$ zone axis. (a) Large view TEM image. (b) Structural model in the [001] zone axis. (c) Details of the nanoparticle arrangements. Scale bar in (a) represents 50 nm.

of the superlattices appear to be systematically along the $[001]_{sl}$ or $[110]_{sl}$ zone axis, the in-plane orientations of different domains are randomly distributed, which indicates the presence of homogeneous nucleation. Samples obtained after slow drying the binary solution with the CdTe:CdSe ratio ~1:6 and 1:8 exhibit a greater preponderance of domains crystallized in the AB_5 structure. These superlattices appear mostly under the form of thin layers (about one to three unit cell heights) oriented on the [001] zone axis. The lateral dimensions and the in-plane orientations of the domains are similar to the *cub*-AB_{13} sample. A typical view of these layers is shown in Figure 4. Under identical conditions, almost no binary superlattices were obtained by slow drying the binary solution with the CdTe:CdSe ratio ~1:1, 1:2, and 1:3. The formation of both *cub*-AB_{13} and AB_5 structures in this system are highly reproducible.

Formation Mechanism. The formation of binary superlattices is a complex process where different driving forces may be involved. One previously suggested possible driving force is the Coulomb interaction between oppositely charged nanoparticles.[20] Electrophoretic mobility measurements demonstrated that semiconductor or metal nanoparticles can be in possession of either positive, negative, or neutral charge, under certain chemical conditions.[20,21] However, the justification of superlattice formation from Coulomb interactions requires the simultaneous presence of nanoparticles carrying charges of opposite signs. Careful measurement of the electrophoretic mobilities were performed separately on both CdTe and CdSe nanoparticle solutions in chloroform. Before the measurement, for both systems, we used ethanol to precipitate the as-synthesized nanoparticles from their crude solutions and centrifugation/precipitation to "wash" the nanoparticles for four times (the same conditions used for preparing BNSLs) before redispersing the nanoparticles into chloroform for measurements. This procedure enables removal of extra unreacted organics and provides similar solution environments for these two systems of nanoparticles. The results, shown in Figure 5, reveal that both CdTe and CdSe nanoparticles hold a *similar* and *slightly positive* net average charge. These results are consistent with the fact that both the nanoparticles and their capping ligands are quite similar in this case. The residual charge we observed by electrophoretic mobility is attributed to ionization of weakly bound ligands when particles are in dilute chloroform solution. From these measurements we conclude that Coulomb interac-

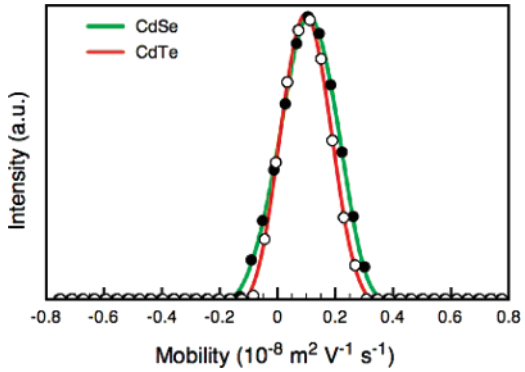

Figure 5. Electrophoretic mobility measurements performed separately on CdTe and CdSe nanoparticle solutions in chloroform.

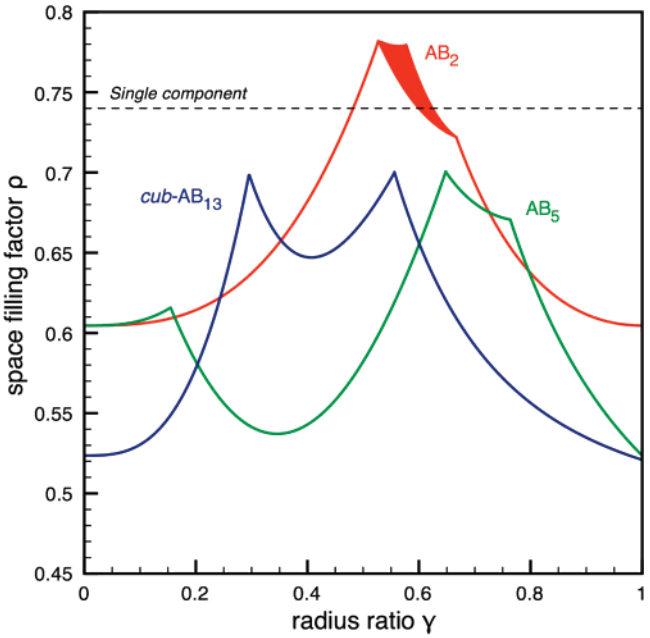

Figure 6. Calculated space-filling curve of AB_5 (isostructural with $CaCu_5$) compared with the curves obtained by Murray and Sanders[2] for *cub*-AB_{13} and AB_2 (isostructural with AlB_2) for the range of radius ratio $0 \leq \gamma \leq 1$. The space-filling factor ($\rho = 0.7405$) corresponding to the single component close-packed structure is indicated by the dotted line.

tions can be excluded as a possible driving force for assembly for the dual semiconductor BNSLs, the superlattices formed are neutral, and we must seek alternative explanations for their formation. Furthermore, in the related field of colloidal crystals in the micrometer scale, where multiple charges can be more precisely controlled, neither *cub*-AB_{13} nor AB_5 appear among the theoretically predicted or experimentally observed structures in systems of oppositely charged particles.[14−17]

Driving Forces: (I) Entropy. A second important possibility is to consider the formation of the binary nanoparticles superlattices as an entropically driven process. Such a process has been well articulated in the dialogue of colloidal assembly and three structures, AB, AB_2, and *ico*-AB_{13}, have been predicted to form in an ideal system of mixed hard spheres by computer simulations.[36−38] In the hard-sphere model, the formation of binary superlattices as a consequence of entropy can be rationalized by distinguishing two types of entropy: the configurational entropy (associated with the degree of spatial ordering) and "free volume" entropy (associated with the space available to each particle to perform local motions).[39] In this kind of approach, the system is expected to adopt the crystal structure corresponding to the most efficient space-filling, i.e., the maximization of the packing fraction ρ for a given ratio of the sphere radii γ.

The simple concept of space-filling curves, developed a long time ago in solid-state chemistry,[40,41] has been successfully used to understand the packing of micrometer-sized silica spheres in gems opals.[2,3] To verify whether such an approach is relevant in our case, we extended the geometrical analysis of Murray and Sanders[2] to the $CaCu_5$ (AB_5) structure. The space-filling curve (ρ versus γ, where ρ = packing fraction and γ = particle radius ratio) for the range $0 \leq \gamma \leq 1$ is shown in Figure 6 together with the curves calculated by these authors for the AB_2 and the *cub*-AB_{13}.

In the case of the AB_5 structure, the first branch of the curve corresponds to the low-γ regime where the lattice parameters a and c of the hexagonal structure are both determined by the A−A contacts and the positions of B spheres are not uniquely defined. For this range of γ, the packing fraction is given by:

$$\rho = \frac{\pi}{3\sqrt{3}}(1 + 5\gamma^3)$$

The upper limit of the branch is reached when the B spheres touch their nearest neighbor A spheres in the basal planes. This contact occurs for $\gamma = 2/\sqrt{3} - 1 \approx 0.1547$. The lattice parameter a is now a function of γ. Accordingly, a second branch corresponding to the packing fraction:

$$\rho = \frac{4\pi}{9\sqrt{3}}\frac{(1 + 5\gamma^3)}{(1 + \gamma)^2}$$

holds until a second contact between the B spheres of adjacent basal planes is reached. This upper bound of the second space-filling curve corresponds to the positive root of the equation:

$$15\gamma^2 - 2\gamma - 5 = 0$$

leading, numerically, to $\gamma \approx 0.6478$. It is important to note here that the highest packing fraction $\rho \approx 0.7005$ is obtained for this specific value of γ. Above this value, the c parameter of the hexagonal unit cell becomes also explicitly dependent on γ. The space-filling curve corresponding to this third configuration is given by:

$$\rho = \frac{8\pi}{9\sqrt{3}}\frac{(1 + 5\gamma^3)}{(1 + \gamma)^2\sqrt{15\gamma^2 - 2\gamma - 1}}$$

The last contact to occur corresponds to the B−B contact in the basal planes of pure B particles ($z = 1/2$). This contact is reached for $\gamma = \sqrt{3}/(4 - \sqrt{3}) \approx 0.7637$. The a lattice parameter is then fully determined by the size of the B particles. The last space-filling curve corresponding to the drastic fall of the packing fraction observed for $\gamma \geq 0.7637$ is given by:

(36) Eldridge, M. D.; Madden, P. A.; Frenkel, D. *Nature* **1993**, *365*, 35−37.
(37) Cottin, X.; Monson, P. A. *J. Chem. Phys.* **1995**, *102*, 3354−3360.
(38) Trizac, E.; Eldridge, M. D.; Madden, P. A. *Mol. Phys.* **1997**, *90*, 675−678.
(39) Hunt, N.; Jardine, R.; Bartlett, P. *Phys. Rev. E* **2000**, *62*, 900.
(40) Laves, F. *Theory of Alloy Phases*; American Society of Metals: Cleveland, OH, 1956.
(41) Parthé, E. *Z. Kristallogr.* **1961**, *115*, 52−79.

$$\rho = \frac{\pi}{6\sqrt{3}} \frac{(1+5\gamma^3)}{\gamma^2\sqrt{15\gamma^2-2\gamma-1}}$$

These results demonstrate that neither *cub*-AB_{13} nor AB_5 binary structures are predicted to be stable on the basis of the space-filling principle, as their packing fractions only reach a maximum of $\rho \approx 0.7$, below the packing fraction ($\rho \approx 0.7405$) obtained for a single component system of hard spheres in either cubic or hexagonal close packing. Moreover, in the case of our study ($\gamma \approx 0.62$), hexagonal AB_2 is the only structure predicted to be stable. Although a bit lower, the packing fraction of *ico*-AB_{13} reaches the value of $\rho \approx 0.70$, which can be further increased by the presence of a slight distribution in the small particle size.[2] The packing fractions of both *cub*-AB_{13} and AB_5 are close to each other around a lower value of $\rho \approx 0.65$ (Figure 6). This analysis leads us to the conclusion that the hard-sphere space-filling principle is a significant feature but is not the sole explanation for the occurrence of these superlattices.

Interestingly, these AB_5 and AB_{13} structures have also been observed in many other systems. *Ico*-AB_{13} as well as AB_5 structures have been reported in the case of binary monodispersed polystyrene latex particles systems of sub-micrometer sizes.[1] *Cub*-AB_{13} and AB_5 structures have also been observed at the nanoscale in oxide−semiconductor[18] and metal−semiconductor binary nanoparticles superlattices.[21] Previously, in BNSLs composed of metal−semiconductor, and oxide−metal nanoparticles, the AB_2 superlattice was observed to coexist with *cub*-AB_{13}.[21,42]

Driving Forces: (II) van der Waals. The space-filling principle does not take into account the ligand shells surrounding the nanoparticles. In nanoparticle superlattice formation, the ligand has contributions in both entropy and the cohesive potential energy:[23,24,43,44] when the overlap between neighboring ligands increases, the orientation entropy of the ligand chains is reduced.[44] By considering *only* the entropic effects from both the hard cores and their soft shells (the ligands), Zilherl and Kamien[44] explained the self-assembly process of soft shell capped hard spheres as a tradeoff between a maximization of the packing fraction (contributed from hard spheres) and a minimization of the interfacial area between neighboring ligand shells. However, Zilherl and Kamien's model does not take into account the van der Waals attraction predicted to occur between the ligand chains. The picture can be understood as follows: when the particles are in relatively dilute solution, the repulsive interaction (due to maximization of the orientation entropy) dominates. But when particles are confined into a shrinking volume (e.g., due to evaporation of the solvent) their surface ligands are ultimately forced to overlap or interdigitate, inducing a VDW attraction (a "freezing" of the ligand structure). The magnitude of this interaction has been overlooked in certain previous models for nanoparticle assembly but could potentially dominate the cohesive energy once ligand shells (e.g., alkyl chains) from neighboring nanoparticles interpenetrate.[23,24,43,45]

To enable further discussion, it is necessary to analyze the extent of ligand−ligand interaction between the shells of the nanoparticles. In this case, the ligands used in the CdTe nanoparticle synthesis include octadecylphosphonic acid (ODPA) and trioctylphosphine oxide (TOPO), whereas in the CdSe synthesis the ligands are stearic acid, TOPO, and octadecylamine (ODA) (see experimental section). Quantitative NMR and IR ligand studies in the literature by similar synthetic methods indicate that even though TOPO is used as one of the capping ligands during synthesis, it is not the primary surface-bound ligand after nanoparticle purification is complete.[33,46,47] Therefore, we deduce that after the purification process the primary surface-bound ligand of the CdTe nanoparticles is ODPA and the primary surface-bound ligands of the CdSe nanoparticles include a combination of stearic acid and ODA. The molecules of both ODPA and ODA contain saturated alkyl chains of 18 carbons (18 C), and the molecule of stearic acid contains a saturated alkyl chain of 17 C. We approximate and model both of the CdTe and CdSe nanoparticles to be hard crystalline cores covered with ligands of saturated alkyl chains composed of ∼18 C.

TEM measurements of the nearest interparticle distance indicate the ligands from two neighboring nanoparticles in both single component and binary superlattices interpenetrate. The average ligand shell thickness of both CdTe and CdSe nanoparticles measured from single component close-packed superlattices is ∼0.8 nm (interparticle distance ≈ 1.6 nm). Measurements of the interparticle distances from the contact directions of the observed *cub*-AB_{13} (B−B contacts for this specific γ) and AB_5 (A-B contacts in the basal planes) structures also confirm this value of ∼1.6 nm. On the basis of the reported C−C bond distance (∼1.54 Å) and the angle value between two C−C bonds (∼110°) of a saturated alkyl chain,[48] we estimate the length of a fully extended alkyl chain of 18 C to be ∼2.1 nm. The nearest interparticle distance in either our single component or binary superlattices is *smaller* (by 5 Å) than the molecular length of ODPA or stearic acid or ODA. On the basis of this compelling experimental data, it is reasonable to assume that the alkyl chain ligands from neighboring nanoparticles interpenetrate (possibly interdigitate). However, the exact configurations of these ligands are not known. In the case of metal nanoparticle self-assembly, the alkyl chains from certain thiol ligands have also been shown to interpenetrate (or possibly interdigitate).[23,24,49] The possible reasons for the smaller core−core separation (than the ligand molecule length) can arise from an increased interpenetration of disordered intercore chains, a large amount of chain packing into the available space away from nearest-neighbor core region, and the formation of chain "bundles".[23]

Considering our nanoparticles as hard crystal cores (of CdTe and CdSe) covered with ligands of saturated alkyl chains composed of ∼18 C, we can estimate the order of magnitude of the two different van der Waals interactions arising between (i) two nearest neighbor particles (e.g., CdTe and CdSe or A−B interaction) (ii) two interdigitating ligand chains. This simplification provides useful qualitative guidance, whereas a full calculation attempting to estimate the total energy of the system is the subject of future research.

(42) Yin, M.; Chen, Z. Y.; Deegan, B.; O'Brien, S. *J. Mater. Res.* **2007**, *22*, 1987−1995.
(43) Salem, L. *J. Chem. Phys.* **1962**, *37*, 2100−2113.
(44) Ziherl, P.; Kamien, R. D. *J. Phys. Chem. B* **2001**, *105*, 10147−10158.
(45) Bain, C. D.; Troughton, E. B.; Tao, Y. T.; Evall, J.; Whitesides, G. M.; Nuzzo, R. G. *J. Am. Chem. Soc.* **1989**, *111*, 321−335.
(46) Peng, Z. A.; Peng, X. G. *J. Am. Chem. Soc.* **2002**, *124*, 3343−3353.
(47) Wang, W.; Banerjee, S.; Jia, S. G.; Steigerwald, M. L.; Herman, I. P. *Chem. Mater.* **2007**, *19*, 2573−2580.
(48) Abrahamsson, S.; Larsson, G.; Vonsydow, E. *Acta Crystallogr.* **1960**, *13*, 770−774.
(49) Motte, L.; Pileni, M. P. *J. Phys. Chem. B* **1998**, *102*, 4104−4109.

The London-van der Waals interaction energy between two spherical systems of respective radii r_1 and r_2 separated by a distance d has been evaluated analytically by Hamaker[50] in the late 1930s. The resulting expression for the mutual energy appears as a function of the nature of the materials constituting the spheres through the Hamaker constant A and the geometry of the system through the radius ratio y ($= r_2/r_1$ of the hard spheres) and the "reduced" interparticle distance x ($= d/2r_1$):

$$E = -A\frac{1}{12}\left\{\frac{y}{x^2+xy+x} + \frac{y}{x^2+xy+x+y} + 2\ln\frac{x^2+xy+x}{x^2+xy+x+y}\right\}$$

In our case, the solvent-retarded Hamaker constants of both $A_{CdTe-CdTe}$ and $A_{CdSe-CdSe}$ in hydrocarbon medium can be estimated to be similar and in the range $\sim 5 \times 10^{-20}$ to 1.2×10^{-20} J ($\sim$0.32 to 0.075 eV).[21,51] A realistic estimation for $A_{CdTe-CdSe}$ is also $\sim$0.32 to 0.075 eV. Combining the value of $A_{CdTe-CdSe}$ and the interparticle separation distance 1.6 nm, the core−core VDW pair interaction energy between our CdTe and CdSe particles in superlattices is ~ -29 to -6.8 meV, which is comparable to the thermal energy k_BT ($\sim$26 meV) at room temperature. Therefore, in our case, the semiconductor core−core VDW interaction is unlikely to be the dominant contribution responsible for superlattice formation.

Another possible contribution to the attractive interaction energy between particles can come from the VDW interaction between neighboring ligand chains. The VDW attraction between two parallel saturated alkyl chains of length L built from N identical basic units ($N\lambda = L$) and separated by a mutual distance D has been evaluated by Salem.[43] In the limit where the distance between chains is much smaller than the molecular length ($D \ll L$), Salem obtained the expression:

$$E = A\frac{3\pi}{8\lambda^2}\frac{L}{D^5}$$

where A is the coefficient of the dispersion interaction between two basic units. Experiments by Ries[52,53] and co-workers have derived the distance D between two stearic acid chains when they are in parallel and form a hexagonal close packing at zero pressure (the cross section area is $\sim (\sqrt{3}/2)D^2$). Using this value ($D \approx 4.8$ Å) Salem evaluated the VDW attraction between two nearest parallel hydrocarbon tails of stearic acid (17 C saturated alkyl chains) in a close-packed configuration to be ~ -8.4 kcal/mol, which is ~ -364 meV/molecule. This value indicates that the ligand−ligand VDW interactions might be an order of magnitude larger than the VDW between the particles themselves once the ligand chains from nearest nanoparticle interpenetrate. Compared to the VDW attraction between two alkyl chains, the repulsive interaction due to overlap of interacting electron clouds begins to be effective only when the D becomes smaller. At $D = 2.94$ Å, the repulsion due to the H−H interaction (H here denotes hydrogen) between two CH_2 units from two neighboring alkyl chains was calculated to be $\sim$0.38 kcal/molecule per CH_2 group (compared to the attraction value at the same D is $\sim$2.09 kcal/molecule per CH_2 group).[43]

The energy between two of our particles in a superlattice (e.g., CdTe interacts with CdSe) due to the ligand−ligand VDW interaction can then be calculated by multiplying the VDW attraction energy per pair of molecule by the number of pairs of interacting molecules. From previous Langmuir−Blodgett (LB) film experiments, the reported zero pressure cross sectional area of stearic acid, ODA, and ODPA are very similar. They are $\sim$0.2 nm^2/molecule,[53,54] 0.19 nm^2/molecule,[55,56] and 0.22 nm^2/molecule,[57] respectively. Since both the alkyl chain length and the cross sectional area of these primary ligands in our system are very similar to stearic acid, we infer the same London-van der Waals interaction energies for this series of ligands (-364 meV/molecule) given similar interchain distance. At this stage of analysis, the evaluation of the interaction energy between two CdTe and CdSe nanoparticles is not possible due to the lack of information on the exact topology of the ligand shells surrounding the particles. Indeed, the great sensitivity to distance of the van der Waals forces requires a precise knowledge of the geometry of the system to produce reliable estimates. For example, the estimation using the cross sectional area derived from the LB film could cause an overestimation of the interaction if the surface bound ligands can only bind to specific sites (e.g., Cd sites). The existence of weakly bound ligands can cause an underestimation of this interaction energy since they are also forced to be "packed" inside the superstructure as the solution dries and thus increasing the number of interacting ligands. Further, even though TOPO is not likely to be the surface bound ligand following purification,[33,46,47] the existence of a small fraction of TOPO at the surface could lower the interligand interaction energy due to the shorter alkyl chain (8 C) and bulkier structure. The large number of ligand chains present in the contact zone allows us to predict that the interaction energy between two particles within the superlattice would be significantly greater than the interaction energy between two individual chains, possibly by an order of magnitude.

Previously, Landman and Luedtke[23] found in the case of assembly of single component gold nanoparticles passivated by alkyl thiols, that the cohesive energy of the gold superlattice is dominated by VDW chain−chain interactions between ligands of neighboring nanoparticles. It remains to be determined whether the alkyl chains of the ligands are disordered or partially ordered near 300 K. Mueggenburg[24] and co-workers suggested VDW ligand−ligand interactions might be the main contributor for the high Young's modulus observed from atomic force microscopy experiments on their 2D gold nanoparticle (capped by alkyl thiol) self-assembled monolayer.

It is clear that the ligand−ligand VDW interaction can be of great importance in nanoparticle self-assembly, even though we have to point out that its strength depends on the specific ligand

(50) Hamaker, H. C. *Physica* **1937**, *4*, 1058−1072.
(51) Striolo, A.; Ward, J.; Prausnitz, J. M.; Parak, W. J.; Zanchet, D.; Gerion, D.; Milliron, D.; Alivisatos, A. P. *J. Phys. Chem. B* **2002**, *106*, 5500−5505.
(52) Ries, H. E.; Kimball, W. A. In *Gas/Liquid and Liquid/Liquid Interface*; Proceedings of the Second International Congress of Surface Activity; Butterworths Scientific Publications: London, 1957; pp 75.
(53) Ries, H. E. *Sci. Am.* **1961**, *204*, 152.
(54) Wang, Y. C.; Du, X. Z.; Guo, L.; Liu, H. J. *J. Chem. Phys.* **2006**, *124*.
(55) Lee, Y. L. *Langmuir* **1999**, *15*, 1796−1801.
(56) Takahashi, M.; Kobayashi, K.; Takaoka, K.; Takada, T.; Tajima, K. *Langmuir* **2000**, *16*, 6613−6621.
(57) Woodward, J. T.; Ulman, A.; Schwartz, D. K. *Langmuir* **1996**, *12*, 3626−3629.

Table 1. Comparison of the Coordination Numbers and the Compositions of the Coordination Polyhedra for the Different Atomic Sites in AB_2, AB_5, and *cub*-AB_{13} Structures with the Reference Single Component Close-Packed Structures

structure	particle[a]	coordination number	composition of the coordination polyhedron
A (fcc, hcp)	A	12	12 A
AB_2	A	20	8 A + 12 B
	B	9	6 A + 3 B
AB_5	A	20	2 A + 18 B
	B_I	12	3 A + 9 B
	B_{II}	12	4 A + 8 B
cub-AB_{13}	A	24	24 B
	B_I	12	12 B
	B_{II}	12	2 A + 10 B

[a] For both AB_5 and cub-AB_{13}, we distinguish the two inequivalent B sites. In the AB_5 structure, the B_I particles belong to the basal $z = 0$ plane and the B_{II} particles to the $z = 1/2$ pure B basal plane. In the cub-AB_{13} structure, the B_I particle is located at the center of the cuboctahedron and the B_{II} form the cuboctahedron.

structures and the interchain distance. When considering nearest neighbor and second-nearest neighbor coordination spheres for a range of structures, it becomes apparent that ligand chains from a particle in a superlattice could not only interact with ligand chains from its nearest neighbors but also reach certain second-nearest neighbors.[23] Such interactions would further increases the cohesive energy and/or stabilize phases ordinarily considered to be unstable when using only the hard-sphere space filling principle.[23] In our experimentally observed BNSLs, some of the second-nearest neighbor separation distances (e.g., the B−B distance in the AB_2 basal plane ($z = 0$) of the AB_5 structure and the B−B distance between adjacent cub-AB_{13} unit cells) are measured to be smaller than the 2-fold length of a 18 C alkyl chain.

One possible outcome of this kind of "hard spheres with sticky soft shells" model in self-assembly is the occurrence of superstructures of high coordination of their atomic sites. High coordination is favored to maximize interligand interaction energy. Indeed, the coordination number in AB_5, *cub*-AB_{13}, and even AB_2 structures is systematically *higher* than in the single component cubic or hexagonal packing in the case of the large particle. The coordination number for the small particle is even slightly larger in AB_5 and cub-AB_{13} than in AB_2. A comparison of the coordination polyhedra for the different atomic sites of these structures is given in Table 1. Analogous to the situation mentioned by Murray and Sanders, the van der Waals interactions may also appear as a factor stabilizing the *cub*-AB_{13} over the denser *ico*-AB_{13} structure, as it increases the number of contacts between spheres.

A number of other factors may play a role in the process of BNSL formation but are however extremely difficult to quantify. These may include the growth kinetics, which may freeze the system before it reaches its configuration of minimum energy, or the dipole−dipole interactions between nanoparticles, which has been recently demonstrated to play an important role in the single component superlattices of semiconductor PbS and PbSe.[22] Finally, other factors such as the nature of the substrate,[20] the deviation of the nanoparticle shape from a perfect sphere, their size distribution,[2] and the nature of the exact configuration of the interpenetrating organic ligands[58] may influence the superlattice formation.

Conclusion

In this work, we demonstrated the formation of binary superlattices by combining two kinds of semiconductor quantum dots. In the specific system of 8.1 nm CdTe and 4.4 nm CdSe nanoparticles, two different superlattice structures, namely *cub*-AB_{13} and AB_5, have been identified using transmission electron microscopy. Electrophoretic mobility measurements clearly exclude a possible ionic interpretation of the formation of these superlattices. There are strong structural similarities with the superlattices predicted to form by entropic effects alone. However, the packing faction of these structures is significantly lower than in the case of *ico*-AB_{13} or AB_2 for this experimental radius ratio. This clearly demonstrates that the formation of these superlattices at the nanoscale cannot be rationalized using only the concept of hard spheres packing. We suggest that interactions between ligand shells through the Van der Waals forces may also play an important role. The formation of these lower packing density *cub*-AB_{13} and AB_5 structures may thus result from a balance between surface contributions (mainly ligand−ligand VDW) and contributions from the hard spheres (mainly hard-sphere space filling). Semiconductor-semiconductor nanoparticle systems appear to be of great potential for structural diversity. Exploration of systems with different radius ratios, different semiconductor cores, or different organic surfactants may indeed result in the formation of other structures (i.e., AB, AB_2, or *ico*-AB_{13}) offering interesting perspectives for generating novel metamaterials with interesting electronic and optical properties.

Experimental Section

Chemicals. Toluene, ethanol, tetrachloroethylene (TCE), 1-Octadecence (ODE), stearic acid (SA), octadecyl phosphonic acid (ODPA), trioctylphosphine oxide (TOPO) (technical grade 90% for CdSe and ReagentPlus 99% for CdTe synthesis), octadecylamine (ODA), CdO, Te, and 1-dodecanethiol were purchased from Aldrich. Trioctylphosphine (97%) was purchased from Strem Chemicals. All chemicals were used as received.

CdTe Nanoparticles. We used a modification of the method developed by Manna et al.[59] and Carbone et al.[60] First, the TOP−Te solution was made by dissolving 0.035 g of Te in 0.313 g of TOP at 250 °C under nitrogen ambience and rapid stirring for at least 3 h until a light-yellow, transparent solution was obtained. This TOP−Te solution was then transferred into a glove box. Then, the Cadmium phosphonate solution was prepared by dissolving 0.035 g of CdO in the mixture of 0.275 g of ODPA and 3.725 g of TOPO in a 25 mL flask at 280 °C under nitrogen and rapid stirring until colorless transparent. Then this Cadmium phosphonate solution was degassed under vacuum at 110 °C for 3 h to ensure removal of the water generated by the reaction of CdO with ODPA. After degassing the solution, the temperature was brought up to 325 °C under nitrogen. Then the TOP−Te solution was taken out from the glove box and rapidly injected into the solution at 325 °C under rapid stirring. The reaction mixture was cooled to 315 °C, and this temperature was maintained for further nanoparticle growth. For 8.1 nm CdTe nanoparticles, the growth time was 6 min and the reaction was stopped by quickly lowering the temperature to below 100 °C, and ~10 mL of anhydrous Toluene was injected when the temperature was around 60 °C. After cooling to room temperature (RT), the CdTe nanoparticles were then precipitated from the crude solution by adding anhydrous ethanol. Precipitated nanoparticles were

(58) Luedtke, W. D.; Landman, U. *J. Phys. Chem.* **1996**, *100*, 13323−13329.
(59) Manna, L.; Milliron, D. J.; Meisel, A.; Scher, E. C.; Alivisatos, A. P. *Nat. Mater.* **2003**, *2*, 382−385.
(60) Carbone, L.; Kudera, S.; Carlino, E.; Parak, W. J.; Giannini, C.; Cingolani, R.; Manna, L. *J. Am. Chem. Soc.* **2006**, *128*, 748−755.

then redispersed into toluene or TCE. Additional wash (by adding ethanol and centrifugation) was needed for four more times to remove extra unreacted organics.

CdSe Nanoparticles. CdSe nanoparticles were synthesized by the method developed by Kim et al.[61] and Li et al.[62] with minor modifications. Typically, 1.0 M TOP−Se solution was made by dissolving Se shots into TOP solution around 80 °C under nitrogen and rapid stirring until a colorless transparent solution was obtained. This TOP−Se solution was then kept in a glove box. In a 50 mL reaction flask, 0.0514 g of CdO was dissolved in 0.455 g of SA under nitrogen and rapid stirring at 280 °C until colorless transparent. After cooling to RT, 16 mL of ODE, 2 g of TOPO, and 2 g of ODA were added. The system was then degassed under vacuum at 110 °C for 3 h to ensure removal of the water generated by the reaction of CdO with SA. After degassing, the system was refilled with Nitrogen and heated to 300 °C under stirring; 2 mL of 1.0 M TOP−Se was then quickly injected into the solution. The temperature of the system was decreased to 280 °C for the growth of nanoparticles. For 4.4 nm CdSe nanoparticles, the growth time was 30 min and the reaction was stopped by quickly lowering the temperature to RT. The precipitation and washing procedure are the same as in the case of CdTe nanoparticles.

Preparation of Binary Superlattices. Binary nanoparticle superlattices (BNSL) were prepared by modifying the methods developed by Redl et al.[18] and Shevchenko et al.[21] During the last washing procedure of the as-synthesized particles, the precipitate was dried under vacuum and weighted to determine how much solution is needed to re-disperse the nanoparticle precipitate into solution ready for the preparation of BNSL. Typically, the concentration of the single-component CdTe and CdSe particles in solution was controlled to ∼2.7 × 10^{14}/mL and ∼16.8 × 10^{14}/mL, respectively. For both systems, we used TCE (with 0.006 volume fraction additive of 1-dodecanethiol) as the solution to disperse the precipitate after the final wash. We found that adding a small amount (0.006 volume fraction) of 1-dodecanethiol into the TCE solution can enhance the formation of BNSLs in the present case. This may due the fact that 1-dodecanethiol is a higher boiling point solvent (bp ≈ 270 °C) compared to TCE (bp 121 °C) and its existence slows the drying rate of the solution during the growth of the BNSL. Seven bottles of binary nanoparticle solution were then made by mixing the CdTe and CdSe single-component solutions according to the concentration ratios of CdTe/CdSe of ∼1:1, 1:2, 1:3, 1:6, 1:8, 1:13, and 1:16. Substrates (TEM Cu grids back with amorphous carbon film) were placed in glass tubes containing 40 μL of binary nanoparticle solution corresponding to these different ratios. These glass tubes were placed in a stand so that they are tilted by 60−70°. These binary solutions on substrates were first allowed to dry under ambience at RT for overnight (∼15 h) so that the solutions became highly concentrated but not yet totally dried on the substrates. Then these solutions were further dried by placing these tubes on a hot stage (∼55 °C) under nitrogen protection at ambient pressure. Superlattices of *cub*-AB_{13} structure were obtained on substrates from binary solution (CdTe/CdSe ≈ 1:13 and 1:16) after drying on the hot stage for ∼16 h. Superlattices of AB_5 structure obtained on substrates from binary solution (CdTe/CdSe ≈ 1:6 and 1:8) after drying on the hot stage for 24 and 54 h.

Characterization. UV−vis spectra of nanoparticle solution were taken on a HP 8453 UV/Visible Spectrophotometer. PL spectra were obtained using a Triax 552 spectrometer with a 2D array CCD detector from Princeton Instrument. Electrophoretic mobility measurements were taken on a Malvern Zetasizer Nano-ZS Test Measurement System. TEM characterization was carried out using a JEOL-100 microscope attached with a CCD camera.

Acknowledgment. S.O. is grateful for support for this project from CAREER Award No. DMR-0348938. This work was also primarily supported by the MRSEC program of the National Science Foundation under Award No. DMR-02113574 and by the DoE, DE-FG02-03ER15463, and the Engineering Physical Sciences Research Council under a doctoral training account (J.M.). We relied on equipment supported by the NSEC program of the National Science Foundation under Award No. CHE-0117752. PL measurements were carried out by Mr. Kin Fai Mak from the Physics Department of Columbia University. We thank him for his help on obtaining these measurements. S.O. thanks S. K. Kumar and J. T. Koberstein for useful discussions.

JA076698Z

(61) Kim, J. I.; Lee, J. K. *Adv. Funct. Mater.* **2006**, *16*, 2077−2082.
(62) Li, J. J.; Wang, Y. A.; Guo, W. Z.; Keay, J. C.; Mishima, T. D.; Johnson, M. B.; Peng, X. G. *J. Am. Chem. Soc.* **2003**, *125*, 12567−12575.